Simulation of Luminosity Monitoring with LUCID in ATLAS

May 8, 2009

Abstract

Monte Carlo simulations are used to characterize the response of LUCID and its performance as a luminosity monitoring system. All results are obtained with a light LUCID geometry made of 32 (instead of 40) Cerenkov tubes read out by photomultipliers.

The luminosity monitoring performance are evaluated using a GEANT3 simulation of the ATLAS detector and a PHOJET simulation of inelastic pp interactions at $\sqrt{s} = 14$ TeV.

When the number of interactions per bunch crossing is less than 2, a method based on empty bunches counting gives an accuracy of 1%. Hit counting can be used for any μ with an accuracy better than 4%.

Contents

2

1   Introduction

This note presents the performance of LUCID as ATLAS luminosity monitoring system. A detailed study of luminosity monitoring in ATLAS with a toy Monte Carlo is reported in [1].

Given a physical process with cross section σ, the average luminosity per bunch crossing is defined as the ratio between the average number of interactions per bunch crossing (μ) and the cross section:

$$\mathcal{L}_{BX} = \frac{\mu}{\sigma} \tag{1}$$

The average bunch luminosity $\mathcal{L}_{BX}$ relates to the instantaneous luminosity L by the bunch crossing frequency ($f_{rev} = 40$ MHz) and the number of filled bunches (n_{BX}):

$$L = \mathcal{L}_{BX} \times f_{rev} \times \frac{n_{BX}}{3564} \tag{2}$$

The task of a luminosity monitor is to be able to provide an estimate of luminosity at any value of μ.

Luminosity monitors in ATLAS are asked to cover a wide range of luminosities, from $L = 10^{27}\ cm^{-2}s^{-1}$ to $L = 10^{34}\ cm^{-2}s^{-1}$ (LHC design). At the lowest value, the ALFA detector [2] will measure absolute luminosity from elastically scattered protons with a goal accuracy of about 3%. A less precise measurement ($10 - 20\%$ accuracy) is foreseen in special beam conditions when absolute luminosity can be determined from the measurement of beam transverse dimensions with a beam separation scan technique. At design luminosity ($n_{BX} = 2808$ bunches), assuming $\sigma_{inel} = 80$ mb (see Table 3), the expected number of inelastic pp interactions per bunch crossing is $\mu \sim 25$.

For luminosity monitoring, two scenarios can be defined. In the *calibration scenario*, luminosity is so low that the probability of having bunches with overlapping interactions is negligible ($\mu << 1$). This sample is needed to calibrate the detector by evaluating the response to a single pp interaction. A *measurement scenario* is any other scenario in which a monitor is asked to provide the luminosity.

The note is divided in two parts. The first part illustrates the geometrical description of LUCID (Section 2) and the study of the detector response (Sections 3 and 4). In the second part (Sections 5), Monte Carlo simulations of the full ATLAS detector are used to study the performance of LUCID as a luminosity monitoring system. The average number of interaction per bunch crossing is extracted from the measurement samples in a wide range of luminosities with several methods and the results are compared with the expected values.

2   Detector description

A realistic simulation of the main LUCID detector elements (vessel, radiator, tubes, optical surfaces, PMTs and cooling system) has been developed in a stand-alone GEANT4 simulation (version 4.7.1p01).

LUCID consists of two detector modules located at a distance of about 17 m from the pp interaction point (IP). Each module is made of twenty aluminum tubes pointing at the IP (see Figure 1).
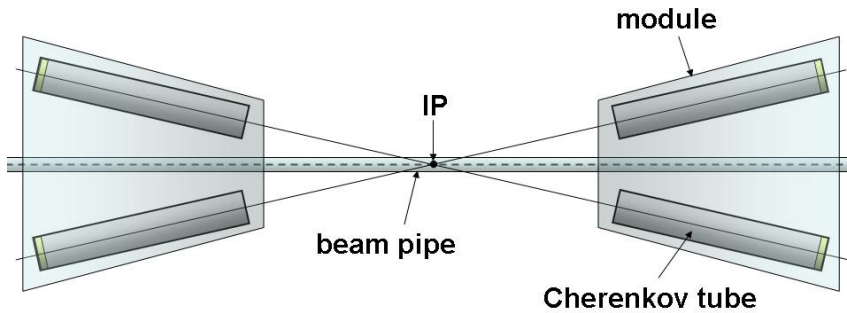
Figure 1. *Schematic view of IP pointing geometry of four LUCID tubes (not in scale).*

Tubes are located in a pressure tight aluminum vessel which contains a Cerenkov gas radiator (C_4F_{10} at 1.1 bar). Sixteen tubes per module are directly coupled to read-out photomultipliers (Hamamatsu R762 PMTs). A cooling system keeps the vessel temperature well below the critical value for a correct behaviour of the PMTs ($50°$ Celsius). Four tubes per module are read-out via optical fibers. A sketch of the geometrical description of a single Cerenkov tube is reported in Figure 2
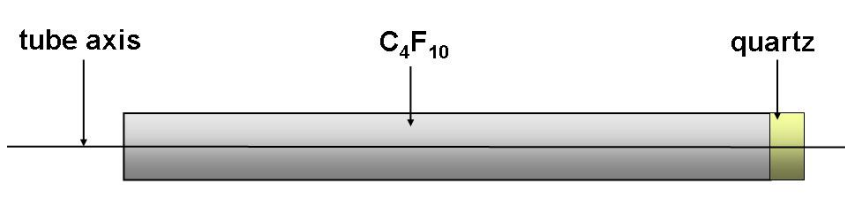
Figure 2. *Geometrical description of the Cerenkov tube (not in scale).*

The PMT is simulated with a thin quartz disc matching the transversal dimension of the tube. The simulation of the PMT quartz window is crucial since it acts as photon emitter, as well as the main gas radiator.

All parameters used to describe the detector geometry are listed in Table 1.

4

Gas pressure [bar]	1.1
Gas temperature [kelvin]	293.15
Distance from the IP [mm]	16715.5
Pmt thickness [mm]	1.2
Pmt radius [mm]	7.0
Tube thickness [mm]	1.0
Tube length [mm]	1495
Tube radius [mm]	7.0
Distance Tube-Beam [mm]	96.3 (ring1), 114.7 (ring2)
Cooling radius [mm]	78
Cooling thickness [mm]	2
Vessel length [mm]	1532
Vessel inner radius [mm]	85
Vessel outer radius [mm]	125.15 (min), 147 (max)
Vessel inner thickness [mm]	2.5
Vessel outer thickness [mm]	3.0
Vessel bulkhead thickness [mm]	3.2

Table 1. *Parameters used for the geometrical description of LUCID.*

2.1 Light emission

Cerenkov light is emitted when a charged particle traverses a material with a speed (v) larger than the speed of light in the medium (c/n)

$$v > \frac{c}{n} \rightarrow \beta = \frac{v}{c} > \frac{1}{n} \tag{3}$$

where n is the refraction index of the radiator. A detailed description of the characteristics of Cerenkov light emission can be found in [3].

The minimal velocity at which Cerenkov emission takes place (c/n) corresponds to an energy threshold (E_{th}) given by

$$E_{th} = \gamma m_0 c^2 = \frac{m_0 c^2}{\sqrt{1 - \left(\frac{v}{c}\right)^2}} = \frac{m_0 c^2}{\sqrt{1 - \left(\frac{1}{n}\right)^2}} \tag{4}$$

where m_0 is the rest mass of the charged particle. The emission angle (θ_C) is a function of the refraction index of the medium:

$$\cos \theta_C = \frac{1}{\beta\, n}. \tag{5}$$

2.1 Light emission

For a gaseous radiator, the refraction index of the material (n) depends on the energy (E) of the emitted photons, on the pressure (P) and the temperature (T) of the radiator, according to the formula

$$n = \sqrt{\frac{2x+1}{1-x}}, \text{ where } x = x(E, P, T) = \frac{KP}{T} \frac{1}{1 - \left(\frac{E}{E_0}\right)^2}.$$ (6)

For C_4F_{10}, when P is in bar, T in kelvin and E in eV, the constants assume the values $E_0 = 17.0$ and $K = 0.25938$. The refraction index of C_4F_{10} and quartz as a function of the wavelength of the emitted Cerenkov light is reported in Figure 3.
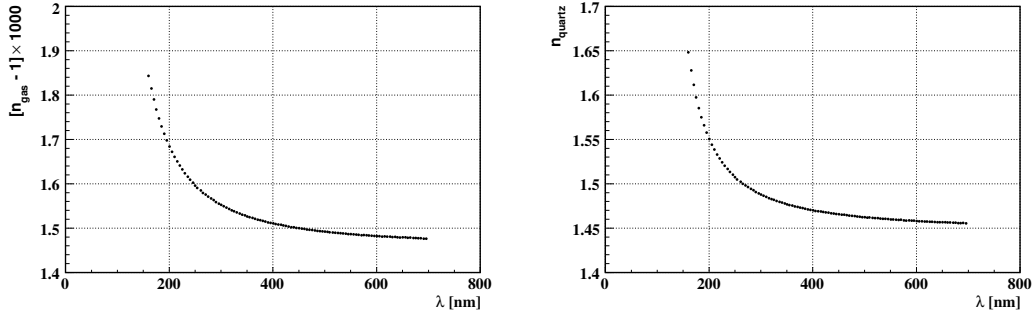
Figure 3. *Refraction index of C_4F_{10} (left) and quartz (right) as a function of wavelength.*

The number of photons emitted per unit of length (L) in the wavelength range $[\lambda_1, \lambda_2]$ has a simple expression in case of long radiators ($L >> \lambda$) [3]:

$$\frac{N}{L[\text{nm}]} = 2\pi\alpha \, \sin^2\theta_C \int_{\lambda_2}^{\lambda_1} \frac{d\lambda}{\lambda^2} = 2\pi\alpha \left[1 - \left(\frac{1}{\beta n}\right)^2\right] \int_{\lambda_2}^{\lambda_1} \frac{d\lambda}{\lambda^2}.$$ (7)

A relativistic charged particle ($\beta \approx 1$) crossing a LUCID tube along its axis at $P = 1.1$ bar, $T = 293.15°$ kelvin emits about 730 photons in the gas and 100 in the quartz in a wavelength range between 200 nm and 700 nm (see Table 2).

	L[mm]	$< n >$	θ_C [°]	E_{th} (π) [MeV]	E_{th} (e) [MeV]	N
C_4F_{10}	1495	1.00149	3.1	2700	9.3	730
Quartz	1.2	1.46	46.8	190	0.7	100

Table 2. Parameters used to calculate Cerenkov photon emission in LUCID.

Density and thickness of the quartz window are such that Cerenkov effect in the PMT is not negligible with respect to that occurring in main LUCID gas radiator.

2.2 Light propagation and detection

After being emitted in C_4F_{10} with a typical angle of $\sim 3°$, photons are reflected by the inner walls of the tube with a certain efficiency (reflectivity). Depending on the position where they are generated, multiple reflections might occur before they actually reach the read-out photomultipliers (see Figure 4).
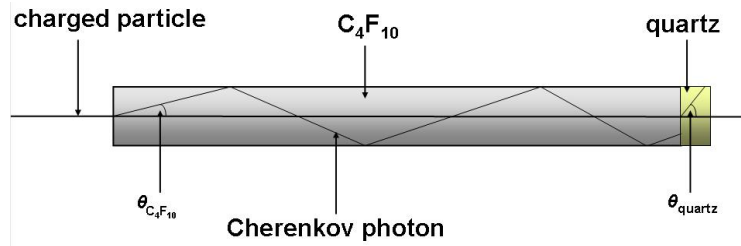
Figure 4. *Light propagation inside a tube.*

The average number of reflections of light in the tube before reaching the PMTs is 2.8. Photons which are not absorbed by the gas reach the end of the tube and are converted by the photomultipliers into photoelectrons. The conversion efficiency (quantum efficiency), which is wavelength dependent, is provided by the manufacturer (Hamamatsu), and is used in the simulation.

Tube reflectivity, which is also a wavelength dependent parameter, and quantum efficiency are used to simulate the propagation and detection of light inside LUCID in the wavelength range accepted by the PMTs [160nm, 650nm] (see Figure 5).

Figure 5. *Aluminum tube reflectivity (left) and PMT quantum efficiency (right) as a function of photon wavelength.*

Gas absorption length is 6 m from 650 to 200 nm and suddenly drops to 1 mm at $\lambda = 150$ nm. For the PMTs, the quantum efficiency contains the wavelength dependence of the absorption length in quartz.

3   Response to single pion events
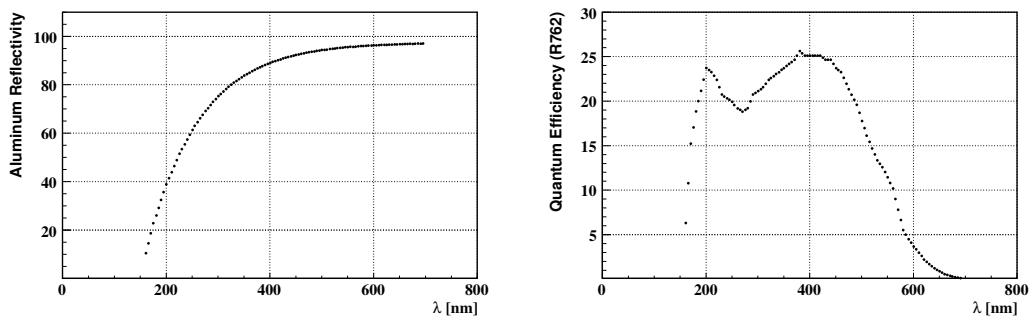
The geometry of LUCID is such that particle originating from the IP (primary) produce more light than particles coming from any other direction (secondaries). The response of LUCID is simulated for particles originating from the IP and traveling exactly along the tube axis (on-axis) or along a random direction (off-axis).

3.1   Signal from on-axis particles

The detector response to 180 GeV charged pions traveling exactly along the tube axis is shown in Figure 6 (left plot), where the number of photoelectrons read-out by the PMTs for every single pion event and for every tube is displayed.
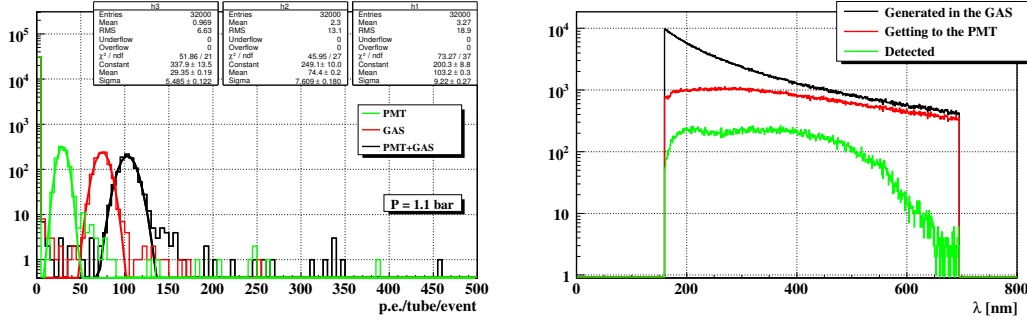
Figure 6. *Left: Photo-electrons per tube per event read-out by LUCID when one pion per event is shot along the tube axis. Right: Wavelength distribution of photons generated by an on-axis charged pion inside a LUCID tube. The distributions of photons propagating up to the PMT and finally detected are superimposed.*

A particle entering the tube and traveling along the tube axis traverses the gas first, and then the quartz window of the photomultiplier. The red histogram, peaked at about 75 photoelectrons, represents Cerenkov light emitted into the gas, whereas photons emitted into the quartz are represented by the green histogram, which shows a maximum at about 30 photoelectrons. The total emitted Cerenkov light is the sum of the two contributions and is peaked at about 105 photoelectrons. Solid lines superimposed to the histograms are the result of the fit. The width is dominated by the Poissonian nature of the photoelectron generation inside the PMT.

The wavelength spectrum of light propagating in LUCID is illustrated in Figure 6 (right plot), at different propagation steps. The wavelength distribution of generated photons (black line) exhibits a $1/\lambda^2$ shape, which is characteristic of Cerenkov emission. Generated photons traverse the gas and are reflected by the aluminum walls of the tube until they reach the quartz window (red line): the suppression at low λ is due to absorption inside the gas and to reduced aluminum reflectivity. The effect of quantum efficiency is visible on the spectrum of detected photons (green line), which are strongly suppressed above 600 nm.

8

3.2   Signal from off-axis particles

In a more realistic scenario, particles originating from pp collisions travel along directions different from the tube axis. In this section, the resonse of LUCID to particles traveling along random directions (off-axis) is studied.

When a primary particle crosses the detector tube walls, secondary particles produced by interaction with the material might cross the Cerenkov radiators (gas or quartz) and release light which will be added to the signal of the original primary particle. The trajectory of secondary particles is typically transverse with respect to the axis of the Cerenkov tube, thus the emission of light is smaller than the one emitted by a primary particle (see Figure 7).
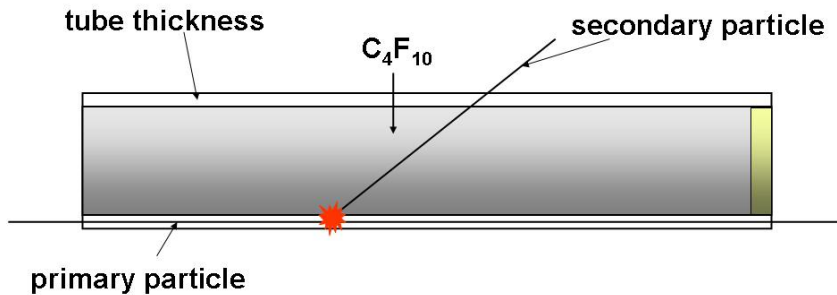
Figure 7. *Path of secondary particles produced in the tube walls.*

Off-axis primary particles are simulated by shooting 180 GeV pions from the IP with a flat polar angle distribution (between 4 and 10 mrad). The resulting photoelectron spectrum is shown in Figure 8, with different assumptions on secondary interactions inside LUCID.
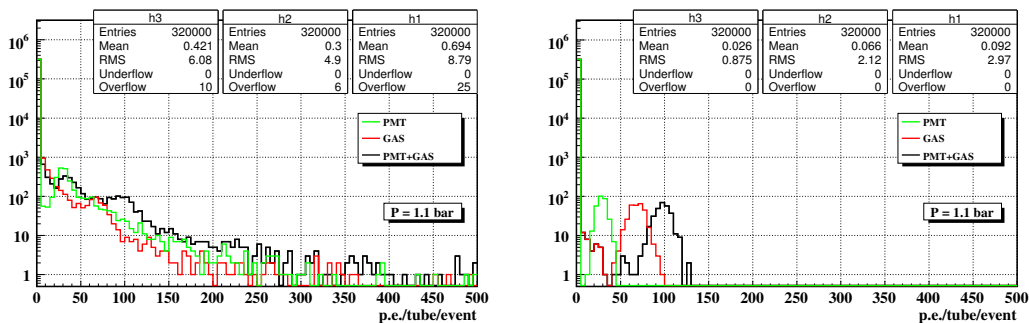
Figure 8. *Photoelectrons produced in LUCID by* 180 *GeV pions originating from the IP along a random direction (left). Right plot shows the effect of neglecting secondary interactions inside the detector material, obtained by reducing the tube walls to zero.*

9

As one can see, the total spectrum of photoelectrons shows two peaks. The peak at about 100 photoelectrons is due to particles, mainly primaries, crossing both Cerenkov radiators (gas and quartz). The peak at 30 photoelectrons originates from particles crossing only the quartz. This is possible only for secondary particles.

Compared to Figure 6, a continuous background is created by secondary particles. Even though tubes are thin ($\approx$ 1 mm), the effective thickness traversed by off-axis primaries is large ($\approx$ 1500 mm), which results in a large probability for secondary interactions. The effect is only partially suppressed by the smaller path length of secondaries inside the Cerenkov radiator.

4 Response to inelastic pp collisions

Inelastic pp collisions at the center of mass energy of 14 TeV are simulated according to the current knowledge of production cross sections and decay branching ratios. Particles are fed through the ATLAS detector simulation to describe the interaction of primary particles with the different detector materials they cross along their path. All primary and secondary particles are finally used as input for the last simulation step in which the performance of LUCID is studied using the standalone simulation described in Section 2. Background originating from beam halo and beam-gas interactions is not simulated. The main features of tracks entering the LUCID volume are compared to those which are detected.

4.1 Event generator

Several packages are available for the simulation of the physics processes occurring in pp collision. The difference among them reflects the uncertainty on the models which are used to describe the interaction of protons. The choice of the generator is not unique. Different generators can be used to evaluate the effect of the different physics models.

The known physics processes which are expected to have larger impact on the performance of LUCID are inelastic pp collisions. There are three types of inelastic events: single-, double- and non-diffractive.

4.1 Event generator

Particles produced in diffractive processes are expected to cluster in specific ranges of pseudo-rapidity (see Figure 10).
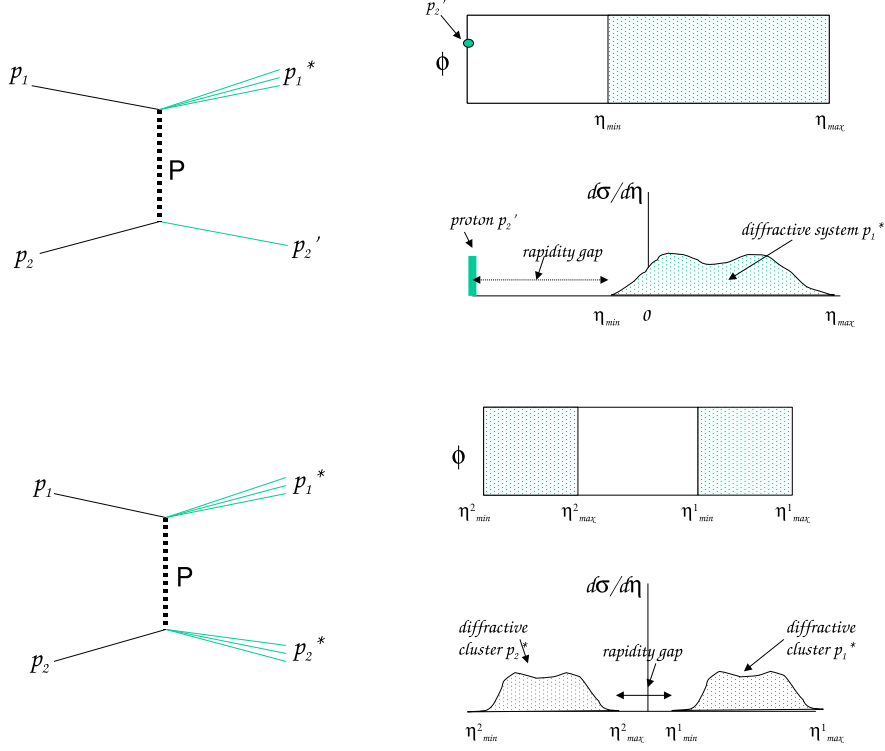
Figure 9. *Illustration of the concept of rapidity gap for single-diffractive (top) and double-diffractive (bottom) processes.*

The production cross section of the different inelastic processes predicted by two generators (PYTHIA and PHOJET) at the center-of-mass energy of 14 TeV are reported in Table 3.

Type of pp collision	σ [mb] in PYTHIA	σ [mb] in PHOJET
Non-diffractive	55.2	64.9
Single-diffractive	14.3	10.8
Double-diffractive	9.7	4.0
Total	79.2	79.7

Table 3. *Cross section of the different inelastic processes (single-, double- and non-diffractive) predicted by PYTHIA and PHOJET [4].*

11

4.1 Event generator

According to both generators, the most frequent inelastic collisions are non-diffractive. The pseudo-rapidity distribution of particles produced in single-, double- and non-diffractive processes predicted by PYTHIA and PHOJET are shown in Figure 10 [4].
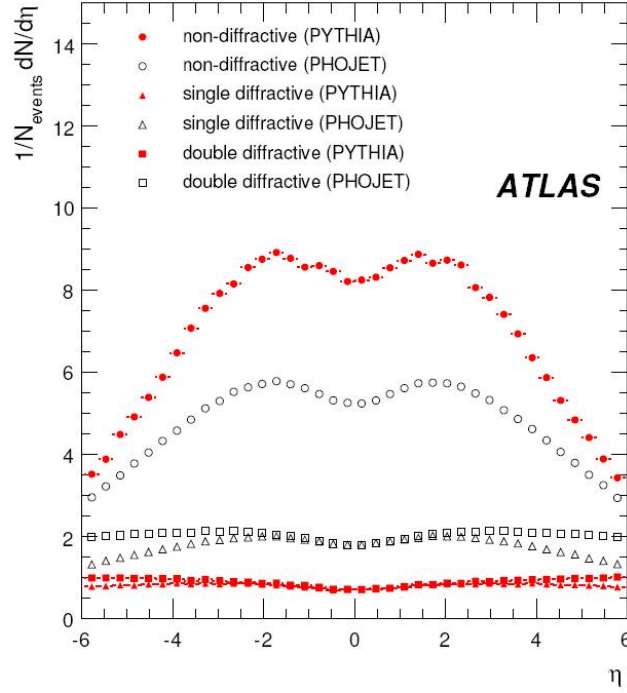
Figure 10. *Pseudo-rapidity distributions predicted by different event generators for different physics processes. Open (close) symbols correspond to PHOJET (PYTHIA).*

The prediction of PYTHIA and PHOJET are close, as far as single- and double-diffractive events are concerned. The largest discrepancies are observed at low values of pseudo-rapidity for non-diffractive events, and over the whole pseudo-rapidity range for single- and double-diffractive events. There is no ground to consider one generator more reliable than the other. The study presented in this thesis is done with a sample of about 10000 events of single pp interactions generated with PHOJET 1.12 in a pseudo-rapidity range $[5.3, 6.1]$.

4.2 Track propagation inside ATLAS

Particles generated by PHOJET 1.12 are fed through a GEANT3 simulation of the ATLAS detector including all sub-systems (magnets, trackers, calorimeters etc.), with the exception of LUCID. The ATLAS detector geometry used in a previous study of radiation background [5] is chosen for the particular attention given to low energetic processes, such as electromagnetic showers, which are essential for the study of radiation background.

Being located close to the beam pipe, upstream of the forward muon shielding, LUCID is exposed to a large flux of secondary particles. In fact, primary particles produced by inelastic pp collisions at the interaction point interact with the material of the experiment producing secondary particles that may reach LUCID from any direction.

The energy threshold for detecting charged particle in LUCID (10 MeV for electrons) is such that the effect of secondary particles might be consistent.

The original idea behind the LUCID design was to build a detector which was even capable to distinguish between primary and secondary particles. Due to the projective geometry of LUCID, primary particles travel longer paths inside a tube compared to secondary particles (see Figure 11). Primary particles are then expected to emit more Cerenkov light than secondaries.
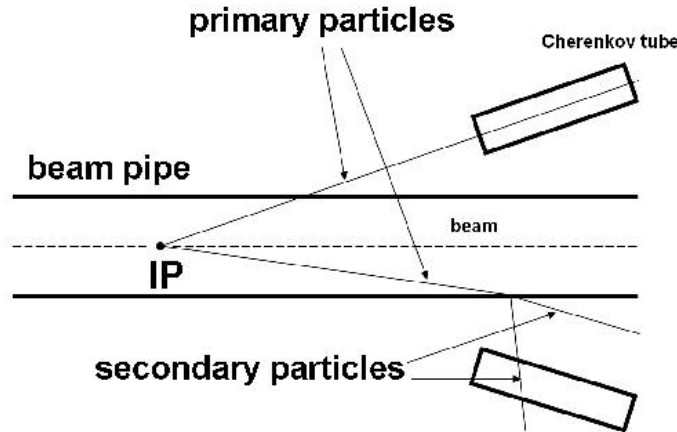

Figure 11. *Schematic view of the paths traveled by primary (solid line) and secondary particles (dashed line). Here the secondaries are due to interaction between the primary and the beam pipe.*

4.3 LUCID volume

The LUCID volume is defined in the region where LUCID is located, reproducing the external vessel where the Cerenkov tubes are contained. The position and the

13

4.3 LUCID volume

four-vector (energy and momentum) of all particles hitting the surface delimiting this volume is recorded, together with the information on the type and the origin (primary or secondary) of the particle. The coordinates of the impact points is shown in Figure 12. The volume is defined in such a way that it contains LUCID but it must not be too large in order not to superimpose to other objects.
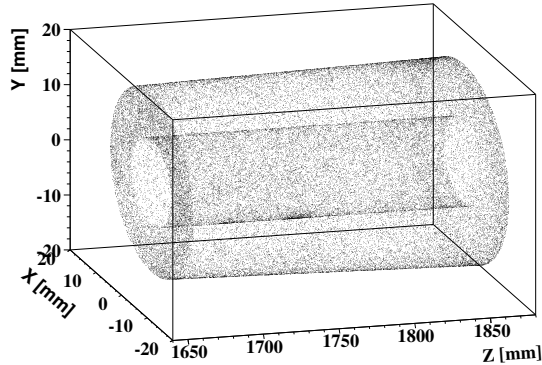
Figure 12. *LUCID volume (z coordinate is along the beam axis).*

One can compare the number of particles generated at the IP with that of primary and secondaries reaching the LUCID volume (seeFigure 13).
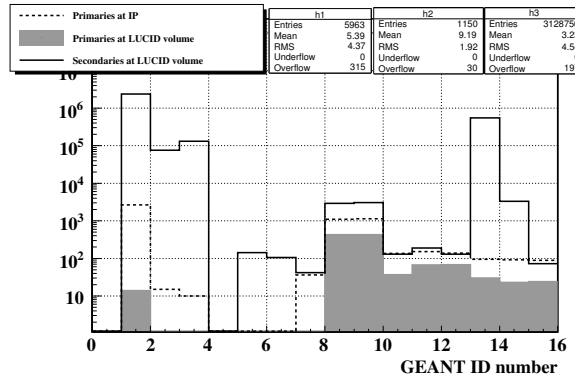
Figure 13. *Distribution of particles generated at the IP (dashed line), primary (filled grey) and secondary particles (solid line) reaching the LUCID volume, according to their GEANT4 identification number.*

The dashed line represents the primary particles produced at the interaction point. They are mostly pions, produced by the interaction of the quarks. The plot shows that a large fraction of primary charged pions travel up to the LUCID volume (filled grey). Photons from $\pi^0 \rightarrow \gamma\gamma$ prompt decays are also labeled as primary particles, but most of them is absorbed before reaching LUCID. The solid line

14

represents the secondary particles reaching the LUCID volume. They are mostly electrons and photons from electromagnetic showers, and neutrons due to back-scattering from the material placed downstream of LUCID.

4.4   Definition of particle direction

The number of photoelectrons produced by a charged particle crossing a LUCID tube is proportional to the path length inside the Cerenkov radiators (gas and quartz). Particles coming from the interaction point and hitting the LUCID volume on the side facing the interaction point are expected to travel the longer path inside the tubes and give the larger contribution of photoelectrons.

In order to study the correlation between the original direction of the particle and the strength of the signal inside LUCID, a direction is associated to each particle. The coordinate of the impact point (x, y, z) and the momentum (p_x, p_y, p_z) of primary and secondary particles allow to define a direction for each particle, even though the criterion is somewhat arbitrary. In this analysis, particles are divided in three classes: front, side and back. If $z \times p_z < 0$, the particle is defined "back". If the particle is not "back" and if $|z| > 16601$ mm, the particle is defined "side". The remaining particles are defined "front".

The z coordinate (the one along the beam axis) of the impact point of all particles on LUCID volume is plotted in Figure 14.
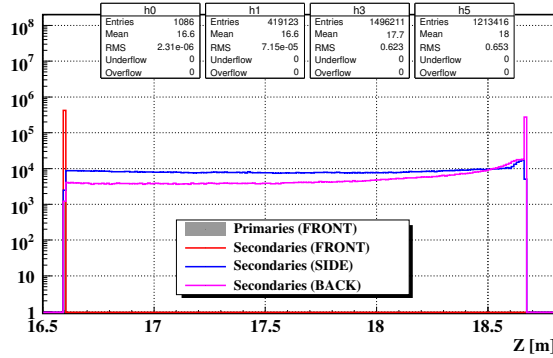
Figure 14. *Distance along the beam axis from the interaction point of the impact point on LUCID. The results are shown for the three classes of particles: "front", "side" and "back" (the definition is given in the text).*

The larger part of "front" particles are secondaries (red line). As expected, "side" and "back" primaries are negligible, and do not appear in the plot. Secondaries not coming directly from the interaction point are mostly "side" (blue line).

4.5   Track propagation inside LUCID

The impact point, the arrival time and the energy at the LUCID volume is used as seed for track propagation inside the volume with the stand-alone GEANT4 simulation presented in Section 2. One important feature of the analysis presented in this chapter is the traceability of the particles. If a particle generates secondaries inside the LUCID detector material, the release of light due to secondaries is associated to the original track.

4.6   Photoelectron spectrum

The response of LUCID to inelastic pp collisions in terms of photoelectrons per tube per event is shown in Figure 15.
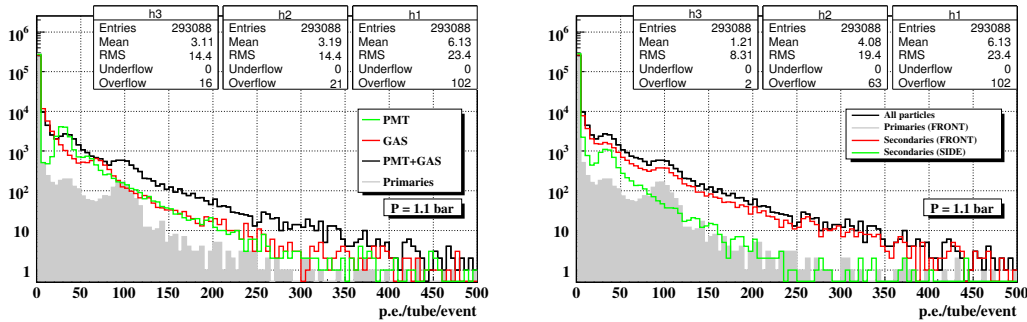
Figure 15. *Spectrum of photoelectrons read-out by LUCID in* 9159 *inelastic pp collisions. Contributions from different radiators (left) and particle directions (right) are shown.*

On the left plot, peaks at the expected positions for production of photoelectrons in the gas (75) and quartz (30) are visible, together with their sum at 105 photoelectrons. Together with the total number of photoelectrons, right plots show three contributions: primary particles (grey area), "front" secondaries (red line) and "side" secondaries (green line).

The spectrum of primary particles is similar to the one shown in Figure 8, which was obtained shooting high energy pions from the IP with a flat polar angle distribution. Compared to those coming from the "front", "side" secondaries travel a smaller path into the tube, thus releasing less Cerenkov light.

4.7   Hit definition

A PMT signal is not always due to Cerenkov light produced by a particle. Light detection related effects, such as dark current and thermoionic emission, may generate noise photoelectrons which can be rejected by setting a threshold, provided that signals of "real" particles are not rejected.
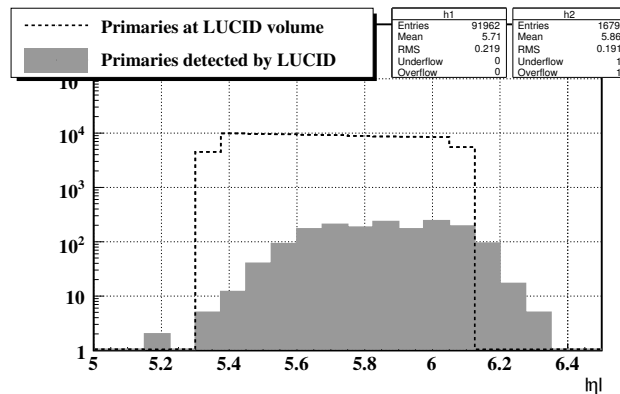
The average number of photoelectrons produced by an on-axis primary particle is about 105 (Figure 6). The largest fraction of secondaries release light in the PMT only (30 photoelectrons). A cut-off threshold of 50 photoelectrons allows to keep the entire signal of primary particles, while suppressing large fraction of secondaries which are not directly correlated with primary particle. A LUCID hit can be defined as a release of light in a tube larger than 50 photoelectrons.

The main features of tracks entering the LUCID volume are compared to those of tracks detected by LUCID when a signal of at least 50 photoelectrons is registered.

4.8 Pseudo-rapidity

The LUCID tubes cover the pseudo-rapidity range [5.61, 5.92]. In Figure 16, the pseudo-rapidity of generated primary particles is compared to that of particles detected in LUCID.

	h1		h2	
	Entries	91962	Entries	1679
	Mean	5.71	Mean	5.86
	RMS	0.219	RMS	0.191
	Underflow	0	Underflow	1
	Overflow	0	Overflow	1

Figure 16. *Pseudo-rapidity distribution of charged primaries generated at the Interaction Point (dashed line) and detected by LUCID (greyed area).*

The pseudo-rapidity of primaries detected by LUCID is calculated using the angle of incidence on the LUCID volume. Due to possible scattering of primaries with the material, this angle can be different from the original angle at the Interaction Point. This effect produces an excess of primaries outside the range of pseudo-rapidity generated at the IP (grey histogram in Figure 16).

In addition, primary particles entering the LUCID volume at pseudo-rapidity values beyond the range of LUCID may generate secondary particles before getting into LUCID, which then enter a tube and release a signal over threshold.

4.9 Time of flight

Particles produced by protons colliding at 14 TeV center of mass energy travel approximately at the speed of light inside the ATLAS detector.

The time needed by primary particles to cover the distance from the interaction point to the front side of LUCID on a straight line is about

$$t \simeq \frac{distance\ between\ IP\ and\ LUCID}{speed\ of\ light} = \frac{17\ m}{2.99 \times 10^8\ m/s} \simeq 56\ ns. \quad (8)$$

The time of arrival of secondaries is expected to be longer since they travel longer paths before hitting LUCID. This is especially true for side and back secondary particles.

The time of flight of particles produced at the IP and reaching the LUCID volume is shown in Figure 17.
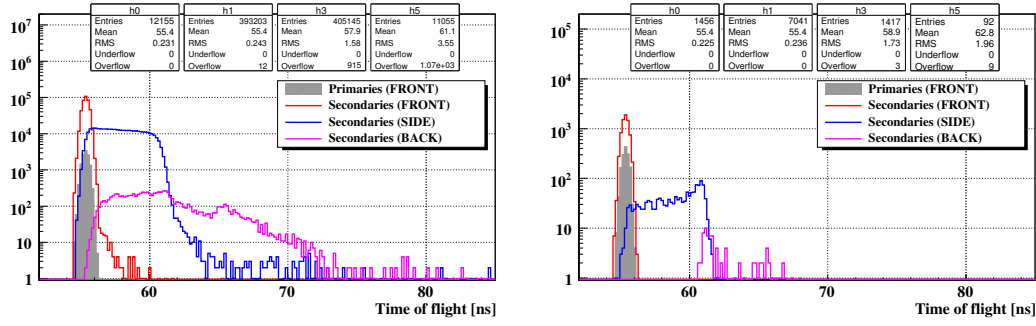
Figure 17. *The left plot shows the time of arrival of all particles from the IP to the LUCID volume. The right plot is the same plot obtained for particles detected by LUCID (> 50 photoelectrons).*

A comparison between the left and right plots shows in particular that most of the detected "side" secondaries traveled a long path before reaching LUCID.

Moreover, the results of the simulation indicate that "front" secondaries are within 2 ns almost in time with primaries, whereas "side" secondaries have a delay of up to 6 ns.

At the moment this thesis is being written, the LUCID collaboration is studying the possibility to upgrade the detector for a Phase II running at LHC design luminosity. One of the proposals to suppress background from "side" secondaries is to apply a time gate on the electronic signal (3 ns coincidence).

4.10 Angle with the beam

Primary and secondary particles hit almost simultaneously the front face of the LUCID volume. However, secondary particles, being the product of scattering of primary particles through different materials, are expected to travel along different directions with respect to primaries.

The angle between the beam axis and the trajectory of primary and secondary particles is shown in Figure 18.
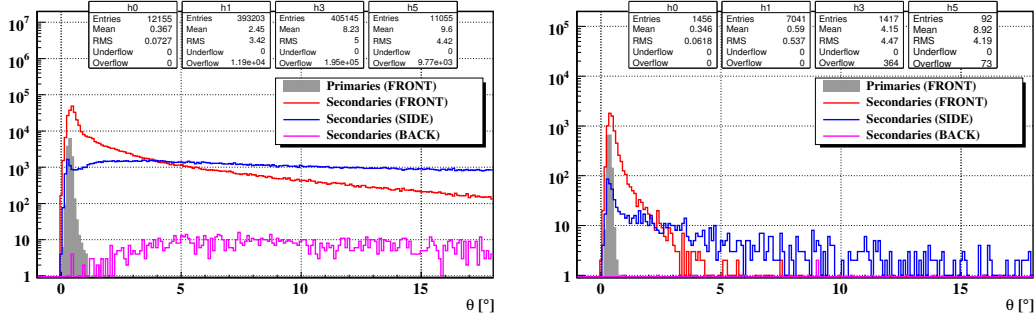
Figure 18. *The left plot shows the angle with the beam axis of particles crossing the LUCID volume. The right plot is the same plot obtained for particles detected by LUCID (> 50 photoelectrons).*

A comparison between the left and right plots shows that "front" and "side" secondaries with angle larger than 2 degrees are both strongly suppressed when arriving at the LUCID volume.

Primary particles form at most an angle of one degree with the beam. The peak of "front" secondaries is broader (two degrees) and the tail extends up to 20 degrees. Within this region, "side" secondaries have a flat angle distribution. Secondaries from the "back" are scattered at larger angles.

4.11 Energy

Most primary particles generated at the IP are pions. Pions are also generated in hadronic showers along the path of primary particles. In Figure 19 the energy distribution of primary and secondary pions are shown.
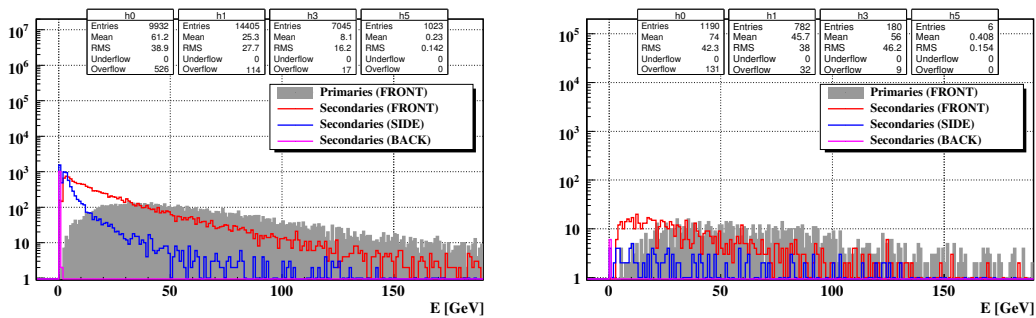
Figure 19. *Energy distribution of pions crossing the LUCID volume (left) and detected by LUCID (right) requiring more than > 50 photoelectrons.*

The requirement of being detected by LUCID suppresses the soft part of the energy spectrum. The average energy of a detected primary pion is 70 GeV, which is close to that of a secondary pion (50 GeV).

19

Secondary particles are mostly photons and electrons. In Figure 20 the energy distribution of secondary particles is shown.

Figure 20. *Energy distribution of photons (top) and electrons (bottom) crossing the LUCID volume (left) and detected by LUCID (right) requiring more than > 50 photoelectrons.*
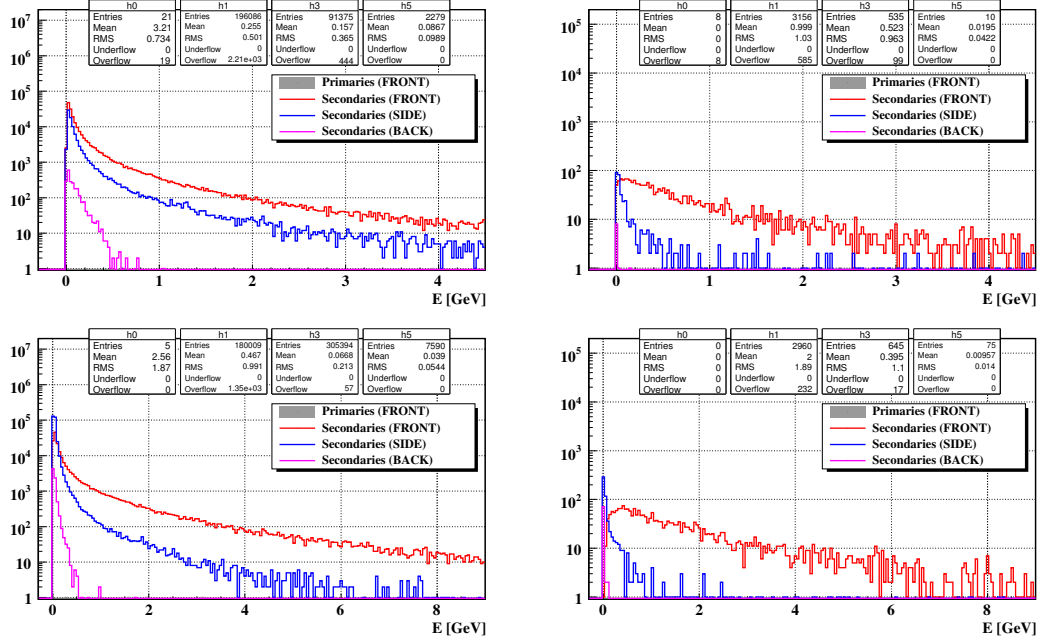
As for pions, the requirement of being detected by LUCID has the effect of suppressing the soft part of the energy spectrum. The average energy of a detected "front" secondary electron is 2 GeV, while "front" secondary photons have 1 GeV. Secondary particles from the "back" are much slower.

5   Simulation of luminosity monitoring

This section is dedicated to the study of the LUCID performance as a luminosity monitoring system.

Monte Carlo simulations of the full ATLAS detector described in Section 4 are used to simulate calibration and measurement scenarios. The calibration sample consists of about 10000 events of single pp interactions. The measurement sample is built by overlapping according to a Poissonian distribution single pp interaction events.

The average number of interaction per bunch crossing (μ_{meas}) is extracted from measurement samples at high luminosity with several methods and the results is compared with the expected value (μ_{true}).

5.1   Definition of detected interaction

LUCID consists of two modules placed symmetrically around the ATLAS interaction point. Two criteria to detect a pp collision are defined: single side mode and coincidence mode. In single side mode, an interaction is detected if there is at least 1 hit in *one module*. In coincidence mode, an interaction is detected if there is at least 1 hit in *both modules* (see Figure 21).
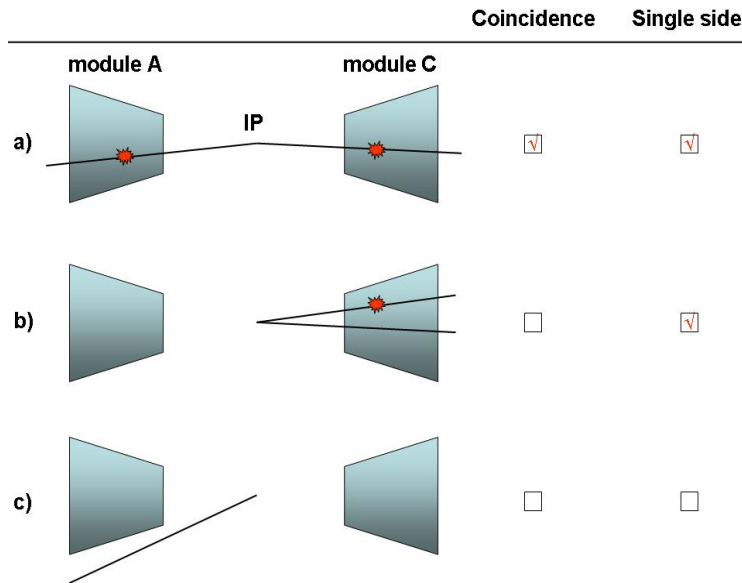
Figure 21. *Principle of detection in single side and coincidence modes.*

In a), each module detects a particle. This interaction is detected both in single side mode and in coincidence mode. In b), two particles traverse the same module, one of them giving a hit. This interaction is detected in single side mode only. In c) no particle traverses any modules, then no interaction is detected.

The advantage of requiring a coincidence is that background produced by beam interactions with residual gas inside the beam pipe or by the beam-halo with LHC collimators is reduced. Since they are uncorrelated with the ATLAS interaction point, such interactions are detected in one module only.

5.2   Detection efficiency and hit distribution

The calibration sample is used to extract the detection efficiency and the average number of hits per pp collision. Efficiency and number of hits depend on the criteria used to define a hit.

In single side mode, the efficiency is $(55.8 \pm 0.05)\%$. In coincidence mode, the efficiency is $(13.5 \pm 0.04)\%$.

The average number of hits per collision is 1.21 ± 0.02 in single side mode, and 0.49 ± 0.01 in coincidence mode. The smaller value in coincidence mode is due to the smaller probability of having a hit simultaneously in both modules.

For each tube, the probability of registering at least one hit is $(3.66 \pm 0.01)\%$, more or less independently of the tube position. This value can also be obtained by dividing the average number of hits per collision in single side mode by the number of tubes (32). Hit multiplicity and tube hit probability are reported in Figure 22.
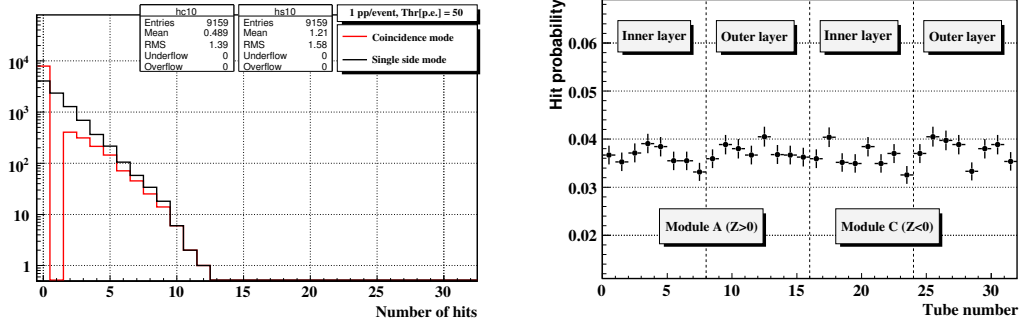
Figure 22. *Number of hits registered by LUCID (left) and hit probability (right) per pp interaction, with a threshold of 50 photoelectrons.*

The efficiency to detect an interaction in single side mode (ε^{Sing}), coincidence mode (ε^{Coin}), in side A (ε^A) and side C (ε^A) and the corresponding average number of hits per interaction are reported in Table 4.

		ε [%]	$N_{hits/pp}$
Single Side	ε^{Sing}	55.8 ± 0.5	1.21 ± 0.02
Coincidence	ε^{Coin}	13.5 ± 0.4	0.49 ± 0.01
Module A	ε^A	34.3 ± 0.5	2.57 ± 0.02
Module C	ε^C	35.0 ± 0.5	2.53 ± 0.02

Table 4. *Efficiencies and average number of hits per interaction.*

Efficiencies for side A and side C include the coincidences; in other words, they represent the probability of detecting and interaction regardless of what happens on the other module.

5.3   Simulation of high luminosity events

High luminosity events are built by overlapping single inelastic collisions with a Poissonian distribution with average μ. To cover a wide range of luminosities, 10

5.3   Simulation of high luminosity events

samples are built with $\mu = 0.01, 0.05, 0.1, 1, 2, 5, 10, 15, 20, 25$. In order to increase the statistics, single interactions are used twice in each sample. The detector responses in terms of photoelectrons per tube per event for two different luminosity values are shown in Figure 23.
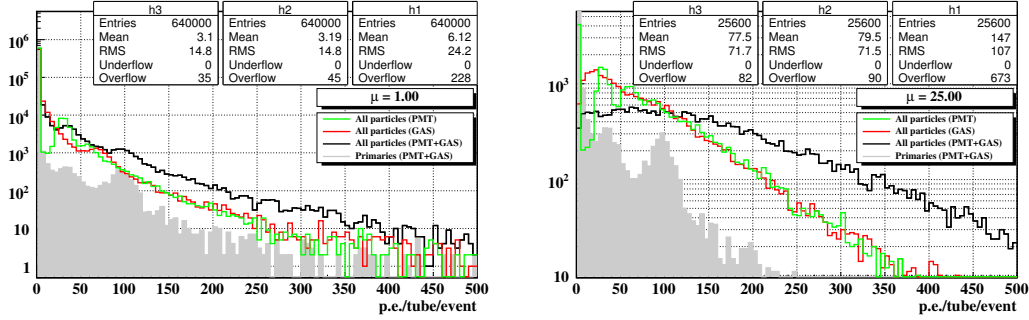
Figure 23. *Photoelectron spectra when $\mu = 1$ (left) and $\mu = 25$ (right).*

The average number of photoelectrons per tube per event increases from 6.1 to 147, when μ goes from 1 to 25. The shape of the total distribution becomes more flat. Due to the increase in track multiplicity, the signal of primary particles is hidden by the combinatorial background of secondaries crossing the tubes at large angles and giving small signals. This effect is called "migration effect". The corresponding hit distributions with a cut-off threshold of $50\ p.e.$ is shown in Figure 24.
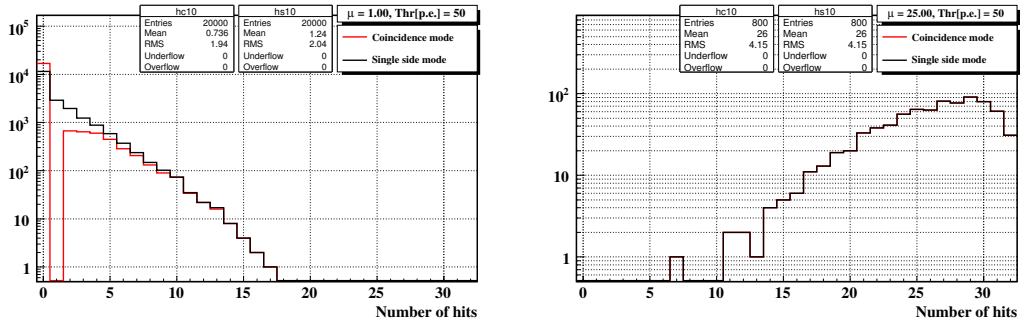
Figure 24. *Hit distribution when $\mu = 1$ (left) and $\mu = 25$ (right), when the cut-off threshold is 50 photoelectrons.*

For $\mu = 1$, the average number of hits per bunch crossing is 1.239 ± 0.008 in single side mode and 0.720 ± 0.006 in coincidence mode. For $\mu = 25$, the hit distributions in single side mode and in coincidence mode becomes indistinguishable. Due to the large detector occupancy, all detected events have at least 1 hit in both modules. The average number of hits per bunch crossing is 25.99 ± 0.08 for both single side and coincidence mode.

23

5.4 Counting methods

The average number of interaction per bunch crossing (μ_{meas}) is extracted from high luminosity samples with several methods and the results is compared with the expected value (μ_{true}).

5.4.1 Zero counting

The basic idea of the zero counting method is to extract μ from the frequency of empty bunches (those without pp collisions). For an ideal detector (100% efficient) in single side mode, the following relation holds (see Equation 13 in appendix A):

$$\mu = -\log(N_{0/BX})$$

where $N_{0/BX}$ is the number of empty bunches. The definition of a empty bunch depends on the definition of detected interaction. In single side mode, empty bunches have 0 hits in both modules. In coincidence mode, empty bunches have 0 hits in at least one module.

The zero counting method has the advantage of simplicity since it relies on counting events rather than hits. A drawback of this method is that the rate of empty events decreases by increasing the luminosity, especially for detectors with large detection efficiency. At design luminosity ($L = 10^{34}\ cm^{-2}s^{-1}$), the number of interactions per bunch is about 25, which implies a rate of empty bunches of $e^{-25} \times 40$ MHz $= 5.6 \times 10^{-4}$ Hz (40 MHz is the crossing rate).

5.4.2 Hit counting

The basic idea of a hit counting method it to extract μ from the number of hits registered by LUCID. Under the assumption that the number of particles in a bunch scales linearly with the number of collisions, the following relation holds:

$$\mu = \frac{N_{particles/BX}}{N_{particles/pp}}$$

n where $N_{particles/BX}$ is the number of particles per bunch and $N_{particles/pp}$ is the number of particles per pp interaction. Under certain assumptions, the number of particles can be turned into hits registered in LUCID using the prescription described in appendix.

The advantage of this method compared to the zero counting method is that it can be used at any luminosity .

5.5   Linear model

In this section an attempt is made to parametrize the response of LUCID (N) with a linear function of μ through the origin:

$$N(\mu) = k_{LUCID} \times \mu$$

The calibration constant (k_{LUCID}) is extracted from the point at $\mu = 0.01$.

5.5.1   Results with zero counting

The linear model with zero counting is tested using the opposite of the logarithm of the fraction of empty events:

$$-\log(N_{0/BX}) = k_{LUCID} \times \mu$$

In Figure 25, the measurements at different μ are compared with the prediction of the linear model, for four values of the threshold ($40, 50, 60, 70$ p.e.).
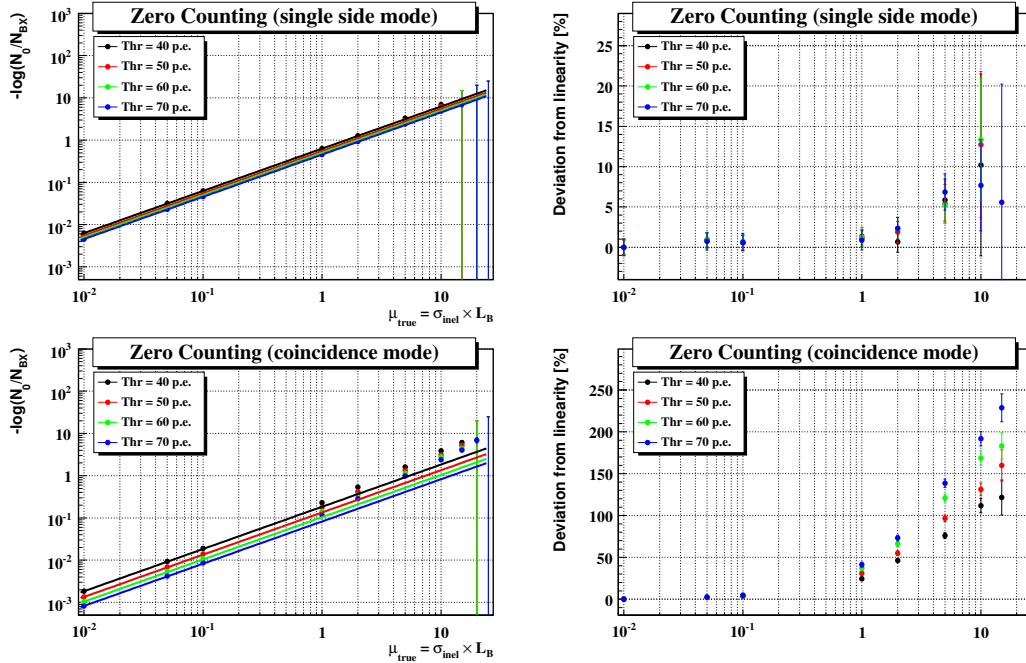
Figure 25. *Comparison between measured LUCID response (dots) and prediction of the linear model (solid line) with zero counting method in single side (top-left) and coincidence mode (bottom-left). The deviation from the prediction is shown in the right plots.*

In single side mode, with a threshold of 50 p.e., the calibration constant is $k_{LUCID} = 0.551 \pm 0.005$ and the deviation from linearity is less than 2% when

5.5 Linear model

$\mu < 2$. In coincidence mode, with the same threshold, $k_{LUCID} = 0.135 \pm 0.002$ and the deviation from linearity is already 4% at $\mu = 0.1$. The deviation from linearity is due to the migration effect. The probability to detect an interaction increases with μ, therefore the number of empty bunches is smaller than the expected one, causing an overestimate of μ. It can be noticed that the calibration constant in single side mode is equal to the detection efficiency (ε^{Sing}, see appendix A).

5.5.2 Results with hit counting

The linear model with hit counting is tested using the number of hits per bunch:

$$N_{hits/BX} = k_{LUCID} \times \mu$$

In Figure 26, the number of hits per bunch at different μ is compared with the prediction of the linear model, for four values of the threshold (40, 50, 60, 70 p.e.).

Figure 26. *Comparison between measured LUCID response (dots) and prediction of the linear model (solid line) with hit counting method in single side (top-left) and coincidence mode (bottom-left). The deviation from the prediction is shown in the right plots.*

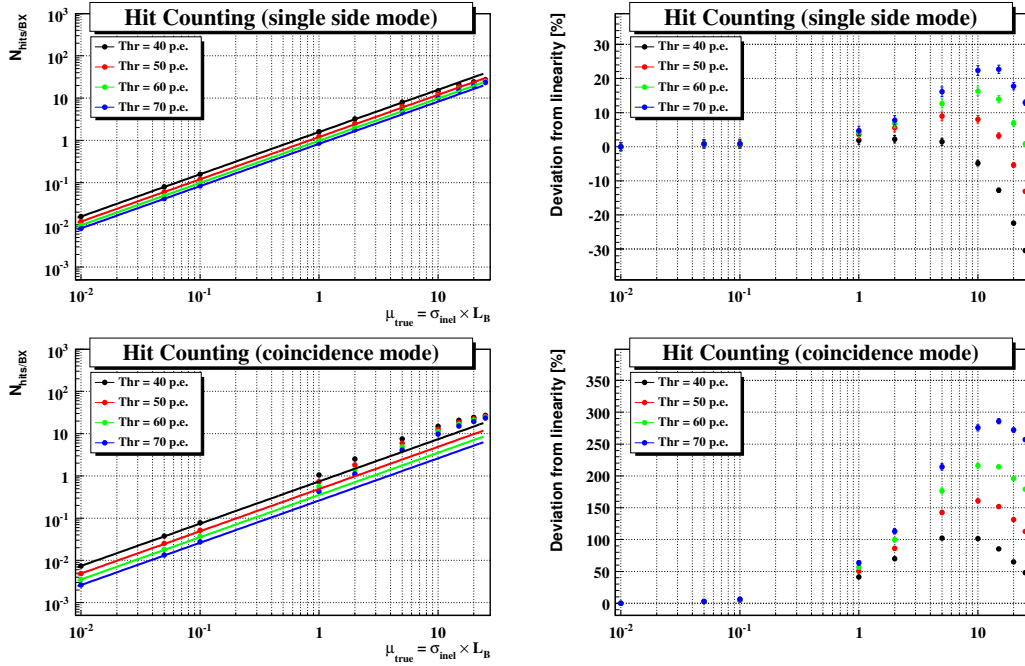In single side mode, with a threshold of 50 p.e., the calibration constant is $k_{LUCID} = 1.120 \pm 0.014$ and the deviation from linearity is 5% when $\mu < 2$. In coincidence mode, with the same threshold, $k_{LUCID} = 0.489 \pm 0.010$ and the deviation from linearity is already 5% at $\mu = 0.1$.

In case of hit counting, the deviation from linearity is due to to effects:

I - Migration effect.

II - Saturation effect;

Migration effect is due to the simultaneous occurrence of signals below thresholds in the same tube. When μ is sufficiently large, small signals can sum up an migrate above threshold. Due to the increase in number of hits, this effect leads to an overestimate of μ at intermediate values $(1 - 10)$.

Saturation effect arise from counting hits instead of particles. In hit counting, the maximum number of hits is limited to the number of tubes (32). When μ is sufficiently large $(\mu > 5)$, the probability of having more particles crossing the same tube become is significant. In these conditions, the number of hits does not increase even though the number of particles increases linearly with μ. Saturation effect leads then to an underestimate of μ.

5.6   Combinatorial model

The response of LUCID at any μ for zero and hit counting ($N_{0/BX}$ and $N_{hits/BX}$) can be analytically computed starting from the information available in single interaction events (detection efficiency and average number of hits per detected event). Calculations are reported in appendix in single side and coincidence mode.

5.6.1   Results with zero counting

In single side mode, the average number of interactions per bunch crossing is related to the fraction of empty bunches by the Equation 13 in appendix A:

$$\mu = -\frac{1}{\varepsilon^{Sing}}\log(N_{0/BX})$$

In coincidence mode, the fraction of empty events is given by Equation 23 in appendix B:

$$N_{0/BX} = f(\mu) = e^{-\mu\varepsilon^A} + e^{-\mu\varepsilon^C} - e^{-\mu(\varepsilon^A+\varepsilon^C-\varepsilon^{Coin})}$$

The average number of interactions per bunch crossing is given by the inverse of $f(\mu)$:

$$\mu = f^{-1}(N_{0/BX}) \tag{9}$$

In Figure 27, the average number of interactions per bunch crossing measured with the zero counting method (μ_{meas}) is compared with the expectation of the combinatorial model, for four values of the threshold $(40, 50, 60, 70$ p.e.$)$.

5.6 Combinatorial model
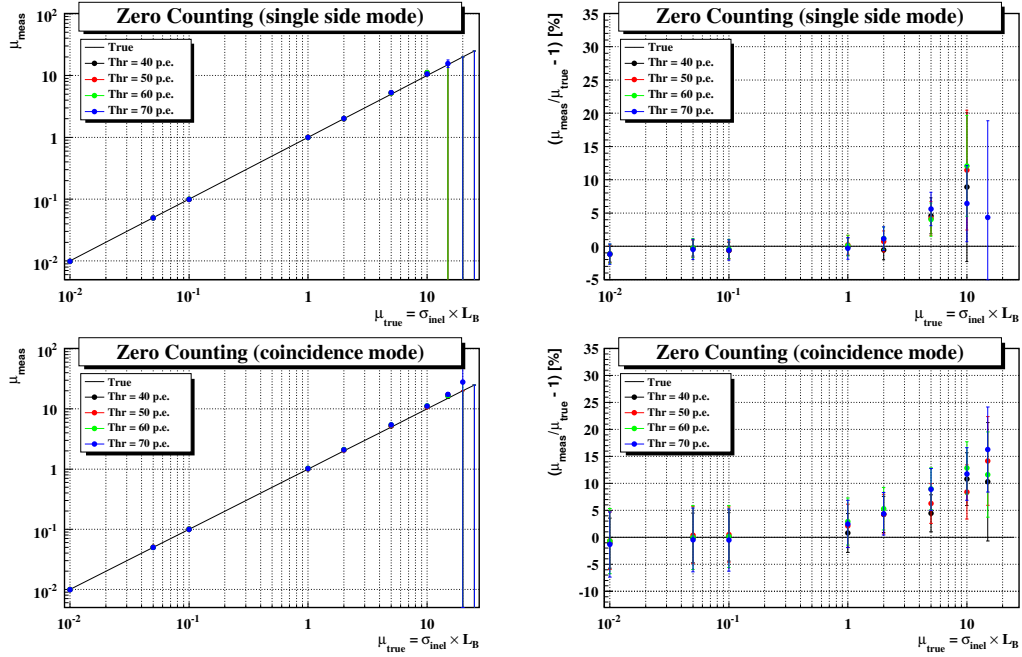
Figure 27. *Comparison between the average number of interactions per bunch crossing measured with LUCID (dots) and predicted with the combinatorial model (solid line) by counting the number of empty bunches in single side (top-left) and coincidence mode (bottom-left). The deviation from the prediction is shown in the right plots.*

In single side mode, for $\mu < 2$, the agreement between the measured and the expected number of interactions is within 1%, when a threshold of 50 p.e. is set. At $\mu = 5$, migration effect starts to play a role. The probability to detect an interaction increases with μ compared to the calibration scenario. The number of observed empty bunch crossings is smaller than the one measured with an ideal detector without migration effect, causing an overestimate of μ.

In coincidence mode, for $\mu < 1$, the agreement between the measured and the expected number of interactions is within 2%, when a threshold of 50 p.e. is set. At $\mu = 2$, migration effect starts to play a role. The probability to detect an interaction increases with μ compared to the calibration scenario. The number of empty crossings is smaller than the expected value causing an overestimate of μ.

In both detection modes, for $\mu > 5$ the statistical uncertainty becomes dominant due to lack of empty events.

5.6 Combinatorial model

5.6.2 Results with hit counting

In single side mode, the average number of pp interactions per bunch crossing can be written as:

$$\mu = \frac{N_{particles/BX}}{N_{particles/pp}}$$

where $N_{particles/BX}$ is the average number of particles per bunch and $N_{particles/pp}$ is the average number of particles per pp interaction.

Trasnforming the number of particles in number of hits registered in the detector according to Equation 46 in appendix D results in:

$$\mu = \frac{\log\left(1 - \frac{N_{hits/BX}}{N_{tubes}}\right)}{\log\left(1 - \frac{N_{hits/pp}}{N_{tubes}}\right)}$$

The number of tubes (N_{tubes}) is 32, while the value of $N_{hits/pp}$ is reported in Table 4.

In coincidence mode, the average number of particles per bunch is give by Equation 43 in appendix C:

$$
\begin{aligned}
N_{particles/BX} \;=\; & \mu C^{Coin}\varepsilon^{Coin}+ \\
& \mu C^{Coin}\varepsilon^{Coin}\left(\frac{C^A\varepsilon^A}{C^{Coin}\varepsilon^{Coin}} - 1\right)\left(1 - e^{-\mu\varepsilon^C}\right) + \\
& \mu C^{Coin}\varepsilon^{Coin}\left(\frac{C^C\varepsilon^C}{C^{Coin}\varepsilon^{Coin}} - 1\right)\left(1 - e^{-\mu\varepsilon^A}\right)
\end{aligned}
$$

The average number of particles (C^A, C^C and C^{Coin}) are defined in Table 8 in appendix C. They are obtained converting the corresponding number of hits defined in Table 4 into particles by using Equation 46 in appendix D. The detection efficiencies (ε^A, ε^C and ε^{Coin}) can be found in Table 4.

In Figure 28, the average number of interactions per bunch crossing measured with the hit counting method in coincidence mode (μ_{meas}) is compared with the expectation of the combinatorial model.
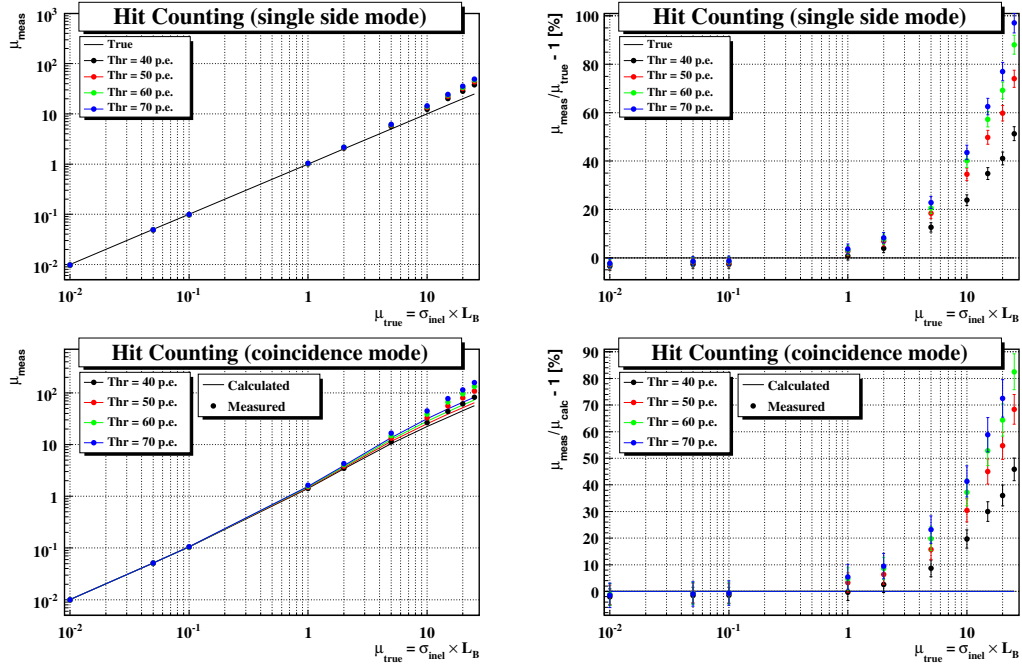
Figure 28. *Comparison between the average number of interactions per bunch crossing measured with LUCID (dots) and predicted with the combinatorial model (solid line) by counting the number of hits in single side (top-left) and coincidence mode (bottom-left). The deviation from the prediction is shown in the right plots.*

In single side mode, for $\mu < 1$, the agreement between the measured and the expected number of interactions is within 2.6%, when a threshold of 50 p.e. is set. For larger values of μ, the disagreement increases exponentially due to migration effect which causes an overestimate of μ.

In coincidence mode, already at $\mu = 1$, the disagreement between the measured and the expected number of interactions is 6%, when a threshold of 50 p.e. is set. For larger values of μ, the disagreement increases exponentially due to migration effect which causes an overestimate of μ.

5.7   Polynomial model

The average number of hits per bunch crossing ($N_{hits/BX}$) has three reasons to be non-linear with μ:

I -   Saturation effect due to hit counting instead of particle counting;

II -   Combinatorial effects arising in coincidence mode;

III -   Migration above threshold of small signals at high μ.

The first two effects have been analytically calculated (see appendix). However, migration effect produces a consistent overestimate of μ already at $\mu = 1$ (for hit counting in coincidence mode) which has not been numerically evaluated.

The accuracy of the luminosity monitor for $\mu > 1$ can be increased by parameterizing all non-linear effects with a polynomial fit:

$$N_{hits/BX} = f(\mu)$$

The inverse of the fit function can be used to evaluate the average number of interactions per bunch crossing corresponding to a given number of hits collected with the detector at any luminosity:

$$\mu = f^{-1}(N_{hits/BX})$$

For this purpose, the Monte Carlo sample is divided into two equal subsets of events. Each set is used to build 10 samples of multiple interaction events by overlapping events according to a Poissonian distribution with average $\mu_{true} = 0.01, 0.05, 0.1, 1, 2, 5, 10, 15, 20, 25$. One samples is used to perform the polynomial fit (calibration sample), the other is used to test the luminosity monitoring performance (measurement sample).

Figure 29 shows the average number of hits per bunch crossing ($N_{hits/BX}$) as a function of the number of interactions μ_{true} in the calibration sample. Results are shown in single side and coincidence mode with four different values of the photoelectron threshold. A third (fifth) order polynomial fit is superimposed to the plot in single side (coincidence) mode. The maximum deviation from the fit is 3% (4%) in single side (coincidence) mode and represents the systematic uncertainty associated to the inversion of the fit function.

Figure 30 shows the average number of interactions extracted from the measurement samples using the inverse of the polynomial fit. At the optimal threshold (50 p.e.), the maximum deviation from linearity is 5% (4%) in single side (coincidence mode) mode.

31

5.7 Polynomial model
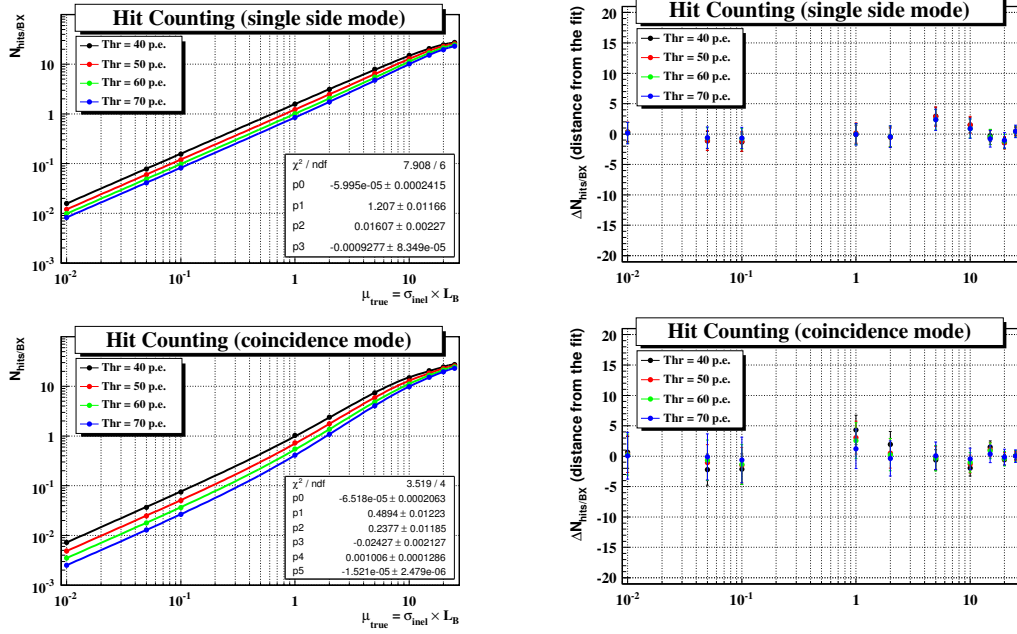
Figure 29. *Polynomial fit of $N_{hits/BX}$ as a function of the true value in single side (top-left) and coincidence mode (bottom-left). The deviation from the fit is shown in the right plots.*
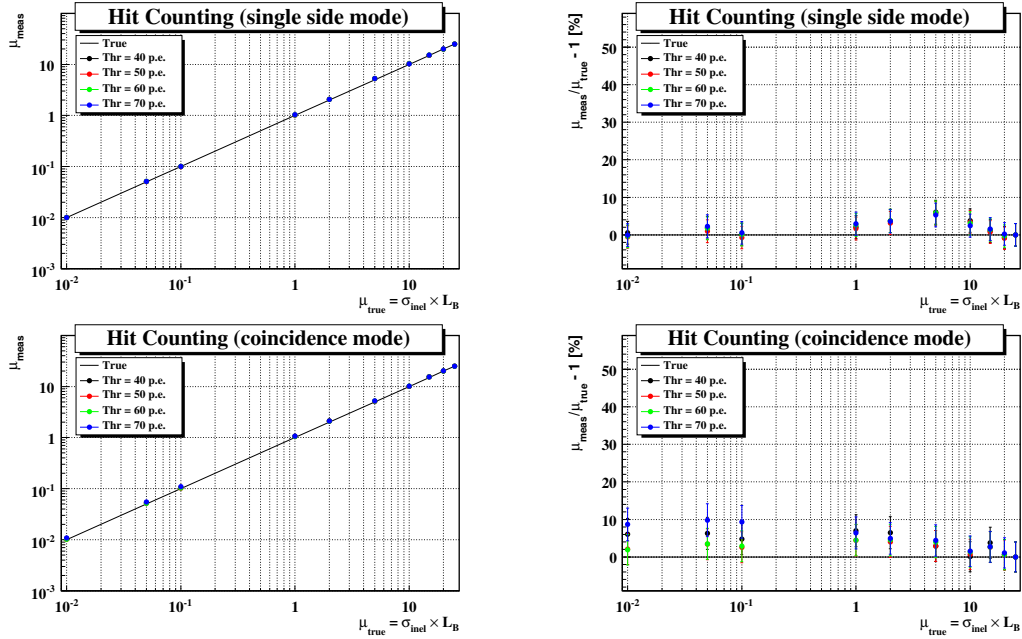
Figure 30. *Comparison between the average number of interactions per bunch crossing measured with LUCID (dots) and predicted with the polynomial model (solid line) by counting the number of hits in single side (top-left) and coincidence mode (bottom-left). The deviation from the prediction is shown in the right plots.*

6   Conclusions

LUCID detects charged particles in the pseudo-rapidity range [5.61, 5.92]. Light yield is 105 photoelectrons in the wavelength range [160nm, 650nm]. The largest fraction of the signal originates from the gas ($\approx$ 75), the rest is coming from the PMT quartz window ($\approx$ 30).

With a cut-off threshold of 50 photoelectrons, the probability to detect inelastic pp collisions is $(55.8 \pm 0.05)\%$, if at least 1 hit in LUCID is required, and $(13.5 \pm 0.04)\%$, when a coincidence between the two detector modules is required. The average number of hits per collision is 1.21.

Three calibration strategies for monitoring luminosity with LUCID based on Monte Carlo simulations are presented. Two alternative counting methods can be used, one based on the detection of empty bunches (zero counting), the other on the number of registered hits per bunch (hit counting). Two alternative modes to detect a pp interaction are foreseen: in single side mode, the interaction is detected if at least one module registers a hit; in coincidence mode, both modules must register a hit. The systematic deviation from linearity of the different methods is reported in Table 5.

Calibration	Counting	Mode	Range	L_{BX} [$10^{30}cm^{-2}s^{-1}$]	σ_{sys}
Linear	Zero	Single Side	$\mu < 2$	< 0.280	2%
Linear	Zero	Coincidence	$\mu < 0.1$	< 0.014	4%
Linear	Hit	Single Side	$\mu < 2$	< 0.280	5%
Linear	Hit	Coincidence	$\mu < 0.1$	< 0.140	5%
Combinatorial	Zero	Single Side	$\mu < 2$	< 0.280	1%
Combinatorial	Zero	Coincidence	$\mu < 1$	< 0.140	2%
Combinatorial	Hit	Single Side	$\mu < 1$	< 0.140	2.6%
Combinatorial	Hit	Coincidence	$\mu < 1$	< 0.140	6%
Polynomial	Hit	Single Side	any	any	5%
Polynomial	Hit	Coincidence	any	any	4%

Table 5. *Systematic uncertainty of luminosity monitoring with LUCID for different methods and range of validity, assuming $\sigma_{pp}^{inel} = 80$ mb.*

Due to the fact that migration effect is not analytically calculated, the combinatorial model is rather inefficient when the number of interactions is larger than 1, independently of the detection mode (single side or coincidence).

For $\mu < 2$, the best method is the combinatorial model in zero counting single side mode (1% accuracy). The advantage of using a polynomial fit is to reach an accuracy of 4% in the whole luminosity range.

A   Counting empty events in single side mode

The probability of having an empty bunch ($N_{0/BX}$) in single side mode is given by two contributions:

I - probability of having 0 interactions;

II - probability of having n interactions with 0 hits in both modules.

Term I is the Poissonian probability of having zero interactions:

$$I = P_\mu(0) = \frac{e^{-\mu}\mu^0}{0!} = e^{-\mu} \tag{10}$$

Given the probability to detect an interaction in single side mode (ε^{Sing}, see Table 4), term II is the combined probability of not detecting the n interactions occurring in a bunch:

$$II = (1 - \varepsilon^{Sing})^n \tag{11}$$

Term II is convoluted with a Poissonian distribution of average μ (the sum starts from $n = 1$ to exclude term I):

$$\sum_{n=1}^{\infty}(1 - \varepsilon^{Sing})^n\frac{e^{-\mu}\mu^n}{n!} = \sum_{n=0}^{\infty}(1 - \varepsilon^{Sing})^n\frac{e^{-\mu}\mu^n}{n!} - e^{-\mu} = e^{-\varepsilon^{Sing}\mu} - e^{-\mu} \tag{12}$$

The probability of observing an empty event is the sum of Equations 10 and 12:

$$N_{0/BX} = e^{-\mu} + e^{-\varepsilon^{Sing}\mu} - e^{-\mu} = e^{-\varepsilon^{Sing}\mu} \tag{13}$$

B   Counting empty events in coincidence mode

The probability of having an empty bunch in coincidence mode is the sum of four contributions:

I - probability of having 0 interactions;

II - probability of having n interactions with at least one interaction detected in module A, together with any number of interactions which are not detected in both modules;

III - probability of having n interactions with at least one interaction detected in module C, together with any number of interactions which are not detected in both modules.

IV - probability of having n interactions with 0 hits in both modules.

The term I is the Poissonian probability of having zero interactions:

$$I = P_\mu(0) = \frac{e^{-\mu}\mu^0}{0!} = e^{-\mu} \tag{14}$$

To evaluate contributions II, III and IV, *exclusive* efficiencies to detect a interaction (ε_1, ε_2, ε_3 and ε_0) are defined in Table 6.

ε_1	probability of detecting an interaction in A, but not in C
ε_2	probability of detecting an interaction in C, but not in A
ε_3	probability of detecting an interaction in both modules
ε_0	probability of detecting no interactions (=$1 - \varepsilon_1 - \varepsilon_2 - \varepsilon_3$)

Table 6. *Efficiencies needed for zero counting method in coincidence mode.*

Exclusive efficiencies in Table 6 are related to the *inclusive* ones defined in Table 4 according to the formula:

$$\begin{aligned}
\varepsilon_1 &= \varepsilon^A - \varepsilon^{Coin} \\
\varepsilon_2 &= \varepsilon^C - \varepsilon^{Coin} \\
\varepsilon_3 &= \varepsilon^{Coin} \\
\varepsilon_0 &= 1 - \varepsilon^A - \varepsilon^C + \varepsilon^{Coin}
\end{aligned} \tag{15}$$

B Counting empty events in coincidence mode

Term II (III) consists of all permutations of k interactions detected in module A (C) and $n - k$ interactions not detected in any module:

$$II = \sum_{k=1}^{n} \varepsilon_1^k \, \varepsilon_0^{n-k} \binom{n}{k} = (\varepsilon_1 + \varepsilon_0)^n - \varepsilon_0^n \tag{16}$$

$$III = \sum_{k=1}^{n} \varepsilon_2^k \, \varepsilon_0^{n-k} \binom{n}{k} = (\varepsilon_2 + \varepsilon_0)^n - \varepsilon_0^n \tag{17}$$

Term IV is the probability of having a bunch crossing with n interactions which are not detected neither by any module singularly nor by the both modules together:

$$IV = \varepsilon_0^n \tag{18}$$

Terms II, III and IV are convoluted with a Poissonian distribution of average μ (the sum starts from $n = 1$ to exclude term I):

$$\sum_{n=1}^{\infty} \frac{e^{-\mu}\mu^n}{n!} \left[(\varepsilon_1 + \varepsilon_0)^n - \varepsilon_0^n \right] = e^{-\mu} \left[e^{-\mu(\varepsilon_1 + \varepsilon_0)} - e^{\mu\varepsilon_0} \right] \tag{19}$$

$$\sum_{n=1}^{\infty} \frac{e^{-\mu}\mu^n}{n!} \left[(\varepsilon_2 + \varepsilon_0)^n - \varepsilon_0^n \right] = e^{-\mu} \left[e^{-\mu(\varepsilon_2 + \varepsilon_0)} - e^{\mu\varepsilon_0} \right] \tag{20}$$

$$\sum_{n=1}^{\infty} \frac{e^{-\mu}\mu^n}{n!} \, \varepsilon_0^n = e^{-\mu}(e^{\mu\varepsilon_0} - 1) \tag{21}$$

The total probability of observing an empty event is the sum of Equations 14, 19, 20 and 21:

$$N_{0/BX} = e^{-\mu(1-\varepsilon_0-\varepsilon_1)} + e^{-\mu(1-\varepsilon_0-\varepsilon_2)} - e^{-\mu(1-\varepsilon_0)} \tag{22}$$

Given the relations in Table 6, Equation 22 can be written as:

$$N_{0/BX} = e^{-\mu\varepsilon^A} + e^{-\mu\varepsilon^C} - e^{-\mu(\varepsilon^A + \varepsilon^C - \varepsilon^{Coin})} \tag{23}$$

C Counting particles in coincidence mode

In coincidence mode, there are two possibilities to detect a bunch with multiple interactions. A *true* coincidence occurs when at least one interaction is detected simultaneously in both modules. A *fake* coincidence occurs when no interaction is detected simultaneously in both modules, but at least two interactions are separately detected in different modules.

In coincidence mode, the average number of detected particles in a bunch with n interactions is the sum of two contributions:

I - the bunch contains at least one interaction which is detected in both modules, together with any number of interactions which are only detected in module A and not in C, and vice versa;

II - the bunch contains 0 interactions detected in both modules, together with at least one interaction which is only detected in module A and one which is only detected in module C.

The average number of particles corresponding to terms I and II is the sum of the probability of each configuration times the corresponding number of detected interactions, times the number of particles per detected interaction.

Four *exclusive* definitions of average number of particles per detected interaction are used (Table 8).

C_1	no. of particles per detected interaction in A, but not in C
C_2	no. of particles per detected interaction in C, but not in A
C_3	no. of particles per detected interaction in both modules
C_4	no. of particles per detected interaction in one module, not in both

Table 7. *Exclusive definitions of average number of particles.*

The probability of each configuration is evaluated by using the efficiencies to detect an interaction defined in Table 6 (ε_1, ε_2, ε_3 and ε_0), together with the efficiency to detect an interaction in one module, but not in both (ε_4).

Suppose n interactions occurred in a bunch crossing, Terms I and II can be written as:

$$I = \sum_{k=1}^{n} \varepsilon_3^k \binom{n}{k} \left[\sum_{l=0}^{n-k} \varepsilon_4^l (1 - \varepsilon_4 - \varepsilon_3)^{n-k-l} \binom{n-k}{l} \right] [kC_3 + lC_4] \qquad (24)$$

$$II = \sum_{k=1}^{n} \varepsilon_1^k \binom{n}{k} \left[\sum_{l=1}^{n-k} \varepsilon_2^l \varepsilon_0^{n-k-l} \binom{n-k}{l} \right] [kC_1 + lC_2] \qquad (25)$$

C Counting particles in coincidence mode

Term I   The first contribution consists of k interactions detected in both modules, l of the remaining $n - k$ interactions detected in only one module and the remaining $n - k - l$ interactions undetected.

The probability of detecting k interactions in both modules is ε_3^k. The probability of detecting l interactions in only one module is ε_4^l. The probability of not detecting $n - k - l$ interactions is $(1 - \varepsilon_4 - \varepsilon_3)^{n-k-l}$.

Binomial factors are used to account for all permutations of k out of n interactions and l out of $n - k$ interactions.

The average number of particles given by k interactions detected in both modules is kC_3, while that of l interactions detected in one module is lC_4.

Term II   The second contribution consists of k interactions detected in module A but not in C, l of the remaining $n - k$ interactions detected in module C but not in A, and the remaining $n - k - l$ interactions undetected.

The probability of detecting k interactions in module A is ε_1^k. The probability of detecting l interactions in module C is ε_2^l. The probability of not detecting $n - k - l$ interactions is ε_0^{n-k-l}.

Binomial factors are used to account for all permutations of k out of n interactions and l out of $n - k$ interactions.

The average number of particles given by k interactions detected in both modules is kC_1, while that of l interactions detected in one module is lC_2.

Sum over l   The l-sums in Equations 24 and 25 can be evaluated by means of the binomial theorem:

$$kC_3 \sum_{l=0}^{n-k} \varepsilon_4^l \, (1 - \varepsilon_4 - \varepsilon_3)^{n-k-l} \binom{n-k}{l} = kC_3(1 - \varepsilon_3)^{n-k} \tag{26}$$

$$C_4 \sum_{l=0}^{n-k} l \, \varepsilon_4^l \, (1 - \varepsilon_4 - \varepsilon_3)^{n-k-l} \binom{n-k}{l} = C_4(n - k)\varepsilon_4(1 - \varepsilon_3)^{n-k-1} \tag{27}$$

$$kC_1 \sum_{l=1}^{n-k} \varepsilon_2^l \varepsilon_0^{n-k-l} \binom{n-k}{l} = kC_1 \left[(\varepsilon_0 + \varepsilon_2)^{n-k} - \varepsilon_0^{n-k} \right] \tag{28}$$

$$C_2 \sum_{l=1}^{n-k} l\varepsilon_2^l \, \varepsilon_0^{n-k-l} \binom{n-k}{l} = C_2(n - k) \, \varepsilon_2(\varepsilon_0 + \varepsilon_2)^{n-k-1} \tag{29}$$

C Counting particles in coincidence mode

Sum over k   Equations 26-29 are used to evaluate the k-sums in Equations 24 and 25 by means of the binomial theorem:

$$C_3 \sum_{k=1}^{n} k\varepsilon_3^k (1 - \varepsilon_3)^{n-k} \binom{n}{k} = C_3 \varepsilon_3 n \tag{30}$$

$$C_4 \varepsilon_4 \sum_{k=1}^{n} n\varepsilon_3^k (1 - \varepsilon_3)^{n-k-1} \binom{n}{k} = C_4 \varepsilon_4 n \left[\left(\frac{1}{1 - \varepsilon_3} \right) - (1 - \varepsilon_3)^{n-1} \right] \tag{31}$$

$$-C_4 \varepsilon_4 \sum_{k=1}^{n} k\varepsilon_3^k (1 - \varepsilon_3)^{n-k-1} \binom{n}{k} = -C_4 \varepsilon_4 n \frac{\varepsilon_3}{1 - \varepsilon_3} \tag{32}$$

$$C_1 \sum_{k=1}^{n} k\varepsilon_1^k (\varepsilon_0 + \varepsilon_2)^{n-k} \binom{n}{k} = C_1 \varepsilon_1 n (\varepsilon_0 + \varepsilon_1 + \varepsilon_2)^{n-1} \tag{33}$$

$$-C_1 \sum_{k=1}^{n} k\varepsilon_1^k \varepsilon_0^{n-k} \binom{n}{k} = -C_1 \varepsilon_1 n (\varepsilon_0 + \varepsilon_1)^{n-1} \tag{34}$$

$$C_2 \varepsilon_2 \sum_{k=1}^{n} n\varepsilon_1^k (\varepsilon_0 + \varepsilon_2)^{n-k-1} \binom{n}{k} = C_2 \varepsilon_2 n \left[\frac{(1 - \varepsilon_3)^n}{\varepsilon_0 + \varepsilon_2} - (\varepsilon_0 + \varepsilon_2)^{n-1} \right] \tag{35}$$

$$-C_2 \varepsilon_2 \sum_{k=1}^{n} k\varepsilon_1^k (\varepsilon_0 + \varepsilon_2)^{n-k-1} \binom{n}{k} = -C_2 \varepsilon_2 n \varepsilon_1 \frac{(1 - \varepsilon_3)^{n-1}}{\varepsilon_0 + \varepsilon_2} \tag{36}$$

Sum of terms I and II   Given that $C_1 \varepsilon_1$ is the number of particles registered in the whole detector when the interaction is detected in module A only and $C_2 \varepsilon_2$ is the number of particles registered in the whole detector when the interaction is detected in module C only, the sum of these terms gives the number of particles registered in the whole detector when the interaction is detected in module A or in module C but not in both:

$$C_4 \varepsilon_4 = C_1 \varepsilon_1 + C_2 \varepsilon_2 \tag{37}$$

Using Equation 37, the sum of Equations 30-36 results:

$$I + II = C_3 \varepsilon_3 n + C_1 \varepsilon_1 n \left[1 - (\varepsilon_0 + \varepsilon_1)^{n-1} \right] + C_2 \varepsilon_2 n \left[1 - (\varepsilon_0 + \varepsilon_2)^{n-1} \right] \tag{38}$$

C Counting particles in coincidence mode

Poissonian sum The average number of particles per bunch is given by the convolution of Equation 38 with a Poissonian of average μ:

$$N_{particles/BX} = \sum_{n=0}^{\infty} (I + II) \frac{e^{-\mu}\mu^n}{n!} \tag{39}$$

Given the relations:

$$\sum_{n=0}^{\infty} n \frac{e^{-\mu}\mu^n}{n!} = \mu \qquad \text{and} \qquad \sum_{n=0}^{\infty} \frac{k^n}{n!} = e^k \tag{40}$$

Equation 39 becomes:

$$N_{particles/BX} = C_3\varepsilon_3\mu + C_1\varepsilon_1\mu \left[1 - e^{-\mu(\varepsilon_2+\varepsilon_3)} \right] + C_2\varepsilon_2\mu \left[1 - e^{-\mu(\varepsilon_1+\varepsilon_3)} \right] \tag{41}$$

The *inclusive* average numbers of particles are defined in Table 8.

C^A	no. of particles per detected interaction in A
C^C	no. of particles per detected interaction in C
C^{Coin}	no. of particles per detected interaction in both modules

Table 8. *Inclusive definitions of average number of particles.*

Using the relations 15 and the following ones:

$$\begin{aligned}
C_1\varepsilon_1 &= C^A\varepsilon^A - C^{Coin}\varepsilon^{Coin} \\
C_2\varepsilon_2 &= C^C\varepsilon^C - C^{Coin}\varepsilon^{Coin}
\end{aligned} \tag{42}$$

Equation 41 can be written as:

$$\begin{aligned}
N_{particles/BX} &= \mu C^{Coin}\varepsilon^{Coin} + \\
&\quad \mu C^{Coin}\varepsilon^{Coin} \left(\frac{C^A\varepsilon^A}{C^{Coin}\varepsilon^{Coin}} - 1 \right) \left(1 - e^{-\mu\varepsilon^C} \right) + \\
&\quad \mu C^{Coin}\varepsilon^{Coin} \left(\frac{C^C\varepsilon^C}{C^{Coin}\varepsilon^{Coin}} - 1 \right) \left(1 - e^{-\mu\varepsilon^A} \right)
\end{aligned} \tag{43}$$

D   From particles to hits

The way particles distribute among the tubes depends on the dynamics of the interactions: single- and double-diffractive, non diffractive etc. Assuming that particles spread uniformly over the detector, the average number of particles hitting one tube is $N_{particles}/N_{tubes}$, where $N_{particles}$ is the total number of detected particles.

Assuming that particles distribute according to a Poissonian, the probability to have at least one particle in a tube, namely a hit, is:

$$1 - e^{-\frac{N_{particles}}{N_{tubes}}} \tag{44}$$

Such probability is turned into number of hits with the following formula:

$$N_{hits} = N_{tubes} \left[1 - e^{-\frac{N_{particles}}{N_{tubes}}} \right] \tag{45}$$

Equation 45 allows to extract the number of particles crossing the detector from the number of hits by using the following relation:

$$N_{particles} = -N_{tubes} \log \left(1 - \frac{N_{hits}}{N_{tubes}} \right) \tag{46}$$

References

[1] S. Ask, *Simulation of Luminosity Monitoring in ATLAS*, ATL-LUM-PUB-2006-001.

[2] ATLAS Collaboration, *ATLAS Forward Detectors for Measurement of Elastic Scattering and Luminosity*, ATLAS TDR 018, CERN/LHCC 2008-04.

[3] J. D. Jackson, *Classical Electrodynamics*, Wiley & Sons, 1975.

[4] ATLAS Collaboration, *Expected Performance of the ATLAS Experiment - Detector, Trigger, Physics*, CERN-OPEN-2008-020.

[5] S. Baranov et al., *Estimation of Radiation Background, Impact on Detectors, Activation and Shielding Optimization in ATLAS*, ATL-GEN-2005-001.